*Acta Cryst.* (1982). A**38**, 143–151

# Application of Two Different Aspherical-Atom Formalisms to Low-Temperature Diffraction Data on Pyridinium-1-dicyanomethylide ($C_8D_5N_3$)*

BY F. BAERT,† P. COPPENS AND E. D. STEVENS

*Department of Chemistry, State University of New York at Buffalo, Buffalo, New York* 14214, *USA*

AND L. DEVOS

*Laboratoire de Dynamique des Cristaux Moleculaires associée au CNRS* (*n*° 465), *Université des Sciences et Techniques de Lille*, 59655 *Villeneuve d'Ascq CEDEX, France*

(*Received* 27 *January* 1981; *accepted* 15 *September* 1981)

## Abstract

Low-temperature (118 K) X-ray data on pyridinium-1-dicyanomethylide have been refined with the aspherical-atom formalism of Hirshfeld [*Isr. J. Chem.* (1977), **16**, 226–230] and the related spherical harmonic expansion proposed by Stewart [*Acta Cryst.* (1976), A**32**, 565–575] as modified by Hansen & Coppens [*Acta Cryst.* (1978), A**34**, 909–921]. The results of the two methods are very similar, except when pseudostatic deformation maps are compared. The triple bond is clearly differentiated from the other bonds, while the ylide carbon atom is neutral. The molecular dipole moment from the multipole formalism is in close agreement with the moment obtained by direct-space integration of the electron density and with the value from solution measurements. On the other hand, the refinement with the Hirshfeld functions leads to a much larger molecular dipole moment. The difference between the two methods in this respect appears to be related to the presence of diffuse monopolar functions in the Hirshfeld expansion.

## Introduction

Deuterated pyridinium-1-dicyanomethylide, $C_8D_5N_3$ (PDM), belongs to the ylide family in which a carbon atom bears a formal negative charge. Its structure was first reported by Bugg & Sass (1965).

Our interest in the electronic structure of PDM stems from its carbanionic character and the associated deviation from planarity at the exocyclic carbon atom [here C(4), Fig. 1]. Stability of the ylides requires that a highly electronegative group is attached to the carbanion. Pyridinium-1-dimethylmethylide, for example, is unstable and cannot be isolated.

We report here the results of two alternative multipole refinements of PDM. The first uses the functions developed and applied by Hirshfeld and coworkers (Hirshfeld, 1977*a*), while the second is based on the spherical harmonic functions as proposed by Stewart (1976), combined with a radial density function which incorporates the expansion–contraction parameter $\kappa$ (Hansen & Coppens, 1978).

Room- and low-temperature neutron diffraction studies of PDM have been reported previously (Devos, Baert & Fouret, 1980).

## Experimental

Deuterated crystals of PDM were grown by slow evaporation of an *N*,*N*-dimethylformamide solution at room temperature. The crystals are light yellow, transparent and mostly platelike. The crystal chosen for data collection shows the forms {111}, {011} and {100} of the monoclinic system and has dimensions of approximately 0·1 × 0·3 × 0·3 mm, the short dimension being perpendicular to the *bc* plane.

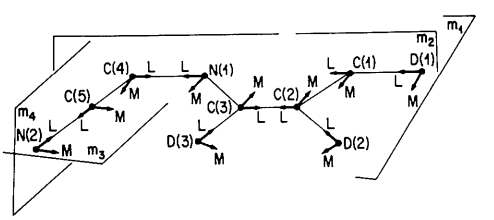


Fig. 1. Numbering of atoms, orientation of local Cartesian coordinate systems and labelling of planes. The plane $m_2$ is a crystallographic mirror plane.

* Electron Population Analysis of Accurate Diffraction Data. XI. Part X: Coppens, Boehme, Price & Stevens (1981).

† Permanent address: Laboratoire de Physique des Solides, Université des Sciences et Techniques de Lille, 59655 Villeneuve d'Asq CEDEX, France.

0567-7394/82/010143-09$01.00

Data were collected at 118 K with Mo $K\alpha$ radiation on a Philips PW 1100 automatic diffractometer, equipped with an Enraf–Nonius gas-flow low-temperature device. Data were scaled with the help of three monitor reflections, the intensities of which decreased slowly by a total of 9% during data collection. Three and two, respectively, symmetry equivalents were collected for $S$ (= $\sin\theta/\lambda$) < 0·6 Å$^{-1}$, and for 0·6 < $S$ < 0·9 Å$^{-1}$, while above 0·9 Å$^{-1}$ only reflections calculated to be observable were measured, up to a limit of $S$ = 1·06 Å$^{-1}$. As the calculated absorption correction varied by at most 1% between reflections, no such correction was made. $R$ factors between symmetry-related reflections defined as $\sum |\langle F^2\rangle - F^2|/\sum F^2$ are 0·0054 for $S$ < 0·4 Å$^{-1}$, 0·0130 for 0·4 < $S$ < 0·9 Å$^{-1}$ and 0·0390 above 0·9 Å$^{-1}$. Crystallographic data are listed in Table 1.*

## Refinements

Three different refinements were carried out, details of which are summarized in Table 2. In the conventional spherical-atom refinement (I) scattering factors for carbon and nitrogen were taken from *International Tables for X-ray Crystallography* (1962), while for deuterium the bonded-hydrogen-atom scattering curve of Stewart, Davidson & Simpson (1965) was used.

* Lists of structure factors for refinements II and III and population parameters for refinements II and III have been deposited with the British Library Lending Division as Supplementary Publication No. SUP 36419 (35 pp.). Copies may be obtained through The Executive Secretary, International Union of Crystallography, 5 Abbey Square, Chester CH1 2HU, England.

Table 1. *Crystal data*

From: Devos, Baert, Fouret & Thomas (1980).

| | |
|---|---|
| Formula | $C_8D_5N_3$ |
| $M_r$ | 148·18 |
| Space group | $P2_1/m$ |
| $\mu$(Mo $K\alpha$) (mm$^{-1}$) | 0·074 |
| $(\sin\theta/\lambda)_{max}$ (Å$^{-1}$) | 1·10 |

Variation in the computed transmission factor $A$ 0·986–0·995

| | 294·5 K | 118 K |
|---|---|---|
| $a$ (Å)† | 7·170 (3) | 7·106 (3) |
| $b$ (Å) | 12·523 (3) | 12·461 (5) |
| $c$ (Å) | 3·878 (1) | 3·802 (1) |
| $\alpha$ (°) | 90·0 | 90·0 |
| $\beta$ (°) | 94·88 | 95·47 |
| $\gamma$ (°) | 90·0 | 90·0 |
| (Mo $K\alpha$) (Å) | 0·7107 | 0·7107 |
| $V$ (Å$^3$) | 346·9 | 335·1 |
| $D_c$ (Mg m$^{-3}$) | 1·418 | 1·468 |
| $Z$ | 2 | 2 |

† Cell dimensions derived by least-squares refinement of 25 reflections with 31 < 2$\theta$ < 42°.

Refinement II is based on the *deformation model* of Hirshfeld which is described in detail elsewhere (Hirshfeld, 1971; Harel & Hirshfeld, 1975; Hirshfeld, 1977*a*). Briefly, the model describes the aspherical atom as the sum of the unperturbed spherical-atom density and a series of deformation functions of the type

$$\rho_{i,n} = P_{i,n}\, N_m\, r^n \exp(-\alpha_i r_i) \cos^n \theta_K, \qquad (1)$$

where $P_{i,n}$ is an adjustable population parameter, $r_i$ is the distance from atomic center $i$, $\alpha_i$ is an adjustable exponent, $N_m$ is a normalization factor, and $\theta_K$ is the angle between a radius vector **r** and a specific polar axis **k**.

Refinement III is based on the spherical harmonic expansion as described by Hansen & Coppens (1978). The model used is a *valence model* as the otherwise unperturbed spherical-atom valence shell is allowed to expand and contract by means of the adjustable scaling parameter $\kappa$. The functional expression for the valence density of atom $i$ is

$$\rho_i = P_{i,\text{valence}}\, \kappa_i^3\, \rho_{i,\text{valence}}(\kappa_i r) + \sum_{l=0}^{n} \sum_{m=-1}^{l} P_{ilm}\, \kappa'^3\, N_{nlm}\, r_i^{n_l} (\exp \alpha_i' r_i)\, y_{ilm\pm}(\theta,\varphi), \qquad (2)$$

where $\rho_{i,\text{valence}}(r)$ is the unperturbed spherical valence shell of atom $i$, the angular functions $y_{ilm\pm}$ are the real spherical harmonics as described, for example, by Kurki-Suonio (1977), the $P$'s are adjustable population parameters and $N_{nlm}$ is a normalization factor. The

Table 2. *Summary of refinements*

| | Spherical atom I | Hirshfeld formalism II | Multipole formalism III |
|---|---|---|---|
| Number of positional variables | 26 | 18* | 18* |
| Number of thermal variables | 52 | 36* | 36* |
| Number of charge-density variables | 0 | 136 | 108 |
| Number of reflections | 2390 | 2391† | 2390 |
| $R$ (all reflections)‡ | 0·073 | 0·028 | 0·029 |
| $R_w$ (all reflections)‡ | 0·098 | 0·035 | 0·039 |
| $S$, goodness of fit§ | 5·8 | 1·71 | 1·85 |
| Scale factor | 15·97 | 15·56 | 15·58 |

* Hydrogen parameters fixed at neutron values.
† Including $F(000)$ for neutrality constraint.

‡ $R = \left\{\frac{\sum|F_o^2 - k^2F_c^2|}{\sum wF_o^2}\right\}$, $R_w = \left\{\frac{\sum w|(F_o^2 - k^2F_c^2)^2|}{\sum wF_o^4}\right\}^{1/2}$.

§ $S = \left\{\frac{\sum w|(F_o^2 - k^2F_c^2)^2|}{n-v}\right\}^{1/2}$, $n$ = number of observations, $v$ = number of variables.

choice of the exponent of $r$, $n_l$, is such as to make the higher spherical harmonic functions more diffuse, as described by Hansen & Coppens (1978). Specifically, $n_l$ is chosen to be 2, 2, 3 and 4 for $l = 1$, 2, 3 and 4 respectively, the rationale for this choice being discussed in the reference.

As described by Hirshfeld (1977*a*), the deformation functions of (1) can be reformulated as a sum of spherical harmonic functions. For $n = 0$ and 1 the $\cos^n \theta_\kappa$ functions are identical to monopolar and dipolar spherical harmonics, respectively, while for higher $n$ they are the sum of spherical harmonics of different order. Thus the six Hirshfeld functions with $n = 2$ are equivalent to five quadrupolar spherical harmonics plus a monopolar function which is more diffuse than the $n = 0$ monopole because of the $r^2$ factor in its radial dependence. When functions through $n = 4$ are included in (1) the expansion consists of three monopoles, two sets of three dipoles, two sets of five quadrupoles, and one set each of seven octapoles and nine hexadecapoles. The Hirshfeld model is thus more flexible than the spherical harmonic expansion (2) because it contains more functions. This difference is somewhat offset by the nonorthogonality of the Hirshfeld functions and the inclusion of the valence-shell expansion and contraction in (2).

For both refinements the number of parameters was reduced by the assumption of local symmetry. In addition to the crystallographic mirror plane passing through atoms D(1), C(1), N(1) and C(4), local mirror planes containing two adjacent atoms were assumed for all heavy atoms with the exception of $C_4$, which is slightly pyramidal. A second mirror plane perpendicular to the first containing the N(2)–C(5) bond ($m_4$ of Fig. 1) was introduced on N(2). Furthermore, identical exponential coefficients and kappas were shared by all hydrogen atoms which were assumed to be cylindrically symmetric with respect to the C–H bond vectors. While the hydrogen expansion was truncated at the dipolar level in the spherical harmonic refinement, terms up to and including $n = 4$ were included in the Hirshfeld model. Hydrogen-atom positional and thermal parameters were kept fixed at the neutron values. With these restrictions the number of parameters listed in Table 2 was obtained for each of the refinements.

Least-squares weights were derived from the estimated standard deviation in the observation, obtained from $\sigma^2(I - B) = I + B + \{0{\cdot}005(I - B)\}^2$. After a number of cycles of refinement an additional term proportional to $F^4$ was added in order to eliminate a remaining dependence of $\sum w(F_o^2 - kF_c^2)$ on $F$ and on $\sin\theta/\lambda$. The proportionality constant was found to be 0·004. In refinement III the total number of electrons was rigidly constrained such that the crystal remained neutral during refinement. In the Hirshfeld program this constraint is introduced by addition of $F(000)$ as an 'observed' reflection with a reasonably large weight. The two procedures proved identical for all practical purposes as $F_{calc}(000)$ agreed with $F_{obs}(000)$ to better than 0·002%. In refinement III extinction was treated isotropically as described by Becker & Coppens (1974), the smallest value of $y$ (defined as $F^2_{corr} = F^2_{obs}/y$) being 0·87. As no extinction treatment is incorporated in the Hirshfeld refinement, refinement III was repeated without the extinction treatment. It was found that this omission at the moderate level of extinction in the present data set did not lead to any significant differences in the refinement results.

## Comparison of results from the two aspherical-atom refinements

### *Agreement factors and structural parameters*

As shown in Table 2, both aspherical-atom refinements lead to a dramatic improvement in the $R$ factors compared with the spherical-atom refinement. A similar improvement is obtained for the goodness of fit. While the unweighted $R$ factor is the same for the spherical harmonic expansion, the weighted agreement factor and the goodness of fit are somewhat less for the Hirsheld expansion, as may be expected on the basis of the larger number of variables in the latter treatment.

A marked *decrease* in scale factor of 2–3% is observed in both refinements, in agreement with earlier experience concerning scale-factor bias which indicated that spherical-atom refinements lead to scale factors which are generally too high compared with high-order results (Steven & Coppens, 1975).

Positional and thermal parameters are given in Tables 3 and 4, while distances between the positions from refinements II (Hirshfeld), III (multipole) and IV (neutron) are listed in Table 5. The differences are small (<0·004 Å) but not quite negligible given the small least-squares standard deviations (0·0008 Å or less). The average discrepancy with the neutron results is about 0·002 Å while the two X-ray results agree somewhat better with each other than with the neutron results (see Table 5). The X-ray results are influenced, of course, by correlation between positional and charge-density parameters. An alternative treatment in which both X-ray and neutron data are refined simultaneously has been described in a previous publication (Coppens, Boehme, Price & Stevens, 1981).

The thermal parameters listed in Table 4 agree between the two X-ray refinements, but are generally higher than the neutron values. This discrepancy, believed to be due, in the present case, to a difference in data collection temperatures has led us to introduce a temperature scaling parameter as a variable in the joint refinement of X-ray and neutron data (Coppens, Boehme, Price & Stevens, 1981). The elimination of

bias in the temperature parameters by the modified X-ray scattering formalism may be judged by the 'rigid bond test' proposed by Hirshfeld (1976). If the amplitudes due to bond-stretching vibrations are small relative to rigid-body displacements the components of atoms $A$ and $B$ along the bond $AB$ should be equal. As shown in Table 6 this criterion is quite closely obeyed in both refinements, the root-mean-square discrepancy being about four and three times a typical estimated standard deviation in the Hirshfeld (II) and multipole (III) refinements, respectively.

Table 3. *Fractional atomic coordinates from the Hirshfeld formalism* (II), *spherical harmonic* (III) *and neutron* (IV) *refinements*

| | | $x$ | $y$ | $z$ |
|---|---|---|---|---|
| C(1) | II | 0·96581 (11) | 0·75 | −0·16003 (12) |
| | III | 0·96561 (7) | 0·75 | −0·15989 (10) |
| | IV | 0·96617 (6) | 0·75 | −0·16018 (14) |
| C(2) | II | 0·87746 (9) | 0·65395 (6) | −0·08664 (9) |
| | III | 0·87737 (5) | 0·65413 (3) | −0·08660 (7) |
| | IV | 0·87753 (5) | 0·65399 (3) | −0·08690 (7) |
| C(3) | II | 0·70694 (11) | 0·65515 (6) | 0·06013 (10) |
| | III | 0·70703 (5) | 0·65532 (3) | 0·06008 (7) |
| | IV | 0·70697 (5) | 0·65527 (2) | 0·05985 (10) |
| C(4) | II | 0·44847 (9) | 0·75 | 0·28785 (15) |
| | III | 0·44857 (7) | 0·75 | 0·28762 (11) |
| | IV | 0·44856 (6) | 0·75 | 0·28745 (14) |
| C(5) | II | 0·36593 (7) | 0·65308 (5) | 0·37690 (9) |
| | III | 0·36604 (5) | 0·65299 (3) | 0·37687 (7) |
| | IV | 0·36626 (5) | 0·65306 (3) | 0·37661 (10) |
| N(1) | II | 0·62302 (13) | 0·75 | 0·13466 (12) |
| | III | 0·62301 (7) | 0·75 | 0·13450 (8) |
| | IV | 0·62312 (4) | 0·75 | 0·13448 (9) |
| N(2) | II | 0·29352 (6) | 0·57406 (5) | 0·45808 (8) |
| | III | 0·29342 (5) | 0·57390 (4) | 0·45816 (7) |
| | IV | 0·29362 (4) | 0·57410 (2) | 0·45787 (9) |
| D(1) | IV | 1·10003 (8) | 0·75 | −0·27386 (21) |
| D(2) | IV | 0·93799 (7) | 0·57699 (4) | −0·14607 (15) |
| D(3) | IV | 0·63511 (6) | 0·58239 (3) | 0·12655 (14) |

Table 4. *Thermal parameter* (Å$^2$ $\times 10^4$) *from the Hirshfeld formalism* (II), *spherical harmonic* (III) *and neutron* (IV) *refinements*

| | | $U_{11}$ | $U_{22}$ | $U_{33}$ | $U_{12}$ | $U_{13}$ | $U_{23}$ |
|---|---|---|---|---|---|---|---|
| C(1) | II | 154 (2) | 212 (2) | 198 (2) | 0 | 39 (2) | 0 |
| | III | 151 (2) | 211 (2) | 199 (2) | 0 | 41 (2) | 0 |
| | IV | 134 (2) | 188 (2) | 167 (2) | 0 | 30 (2) | 0 |
| C(2) | II | 174 (1) | 170 (2) | 209 (2) | 30 (1) | 36 (1) | −11 (1) |
| | III | 174 (1) | 165 (1) | 209 (1) | 30 (1) | 35 (1) | −11 (1) |
| | IV | 150 (1) | 144 (1) | 179 (2) | 26 (1) | 28 (1) | −10 (1) |
| C(3) | II | 169 (1) | 124 (1) | 197 (2) | 6 (1) | 32 (1) | −1 (1) |
| | III | 170 (1) | 118 (1) | 196 (1) | 5 (1) | 31 (1) | −1 (1) |
| | IV | 145 (1) | 100 (1) | 164 (2) | 9 (1) | 22 (1) | −4 (1) |
| C(4) | II | 158 (2) | 126 (2) | 180 (2) | 0 | 33 (1) | 0 |
| | III | 158 (2) | 124 (2) | 180 (2) | 0 | 34 (1) | 0 |
| | IV | 132 (2) | 102 (2) | 153 (2) | 0 | 25 (2) | 0 |
| C(5) | II | 171 (1) | 137 (1) | 206 (1) | −12 (1) | 37 (1) | 11 (1) |
| | III | 172 (1) | 139 (1) | 207 (1) | −13 (1) | 38 (1) | 12 (1) |
| | IV | 146 (1) | 115 (1) | 179 (2) | −10 (1) | 29 (1) | 12 (1) |
| N(1) | II | 142 (2) | 111 (2) | 143 (2) | 0 | 15 (1) | 0 |
| | III | 142 (2) | 112 (2) | 145 (2) | 0 | 16 (1) | 0 |
| | IV | 124 (1) | 97 (1) | 117 (1) | 0 | 4 (1) | 0 |
| N(2) | II | 257 (1) | 163 (1) | 347 (2) | −34 (1) | 91 (1) | 34 (1) |
| | III | 253 (1) | 165 (1) | 341 (2) | −40 (2) | 88 (2) | 36 (2) |
| | IV | 232 (1) | 1142 (1) | 318 (2) | −34 (1) | 79 (1) | 32 (1) |
| D(1) | IV | 226 (2) | 374 (3) | 409 (4) | 0 | 140 (3) | 0 |
| D(2) | IV | 319 (2) | 222 (2) | 434 (3) | 83 (2) | 113 (2) | −32 (2) |
| D(3) | IV | 295 (2) | 147 (1) | 423 (3) | −18 (1) | 113 (2) | 9 (2) |

*Atomic properties: net charges and orbital exponents*

The aspherical-atom results imply values of net atomic charges on all atoms, obtained by the subtraction

$$q_i = Z_i - \sum_{j}^{\text{all monopoles}} P_{ij} - P_{i,\text{core}},$$

where $Z_i$ is the atomic number of atom $i$ and the summation is over the populations of the monopoles only.

The numbers listed in Table 7 show a clear difference between the 'net charges' from the two methods, with the Hirshfeld refinement charges often unrealistically large. This difference must be related to the larger number of, often very diffuse, monopoles in this refinement. This explanation is supported by examination of the atomic dipole moments (not reproduced here), very large positive values for the ring atoms C(2) and C(3) being balanced by very large dipoles in the opposite direction on the adjacent hydrogen atoms. The concept of locality of the electrons (Kurki-Suonio, 1968) is no longer main-

Table 5. *Distances* (*in* Å $\times 10^4$) *between atomic positions from X-ray refinements* II *and* III *and refinement of neutron data* (IV)

| | II/IV | III/IV | II/III |
|---|---|---|---|
| C(1) | 27 (9) | 42 (6) | 16 (9) |
| C(2) | 13 (5) | 24 (5) | 23 (9) |
| C(3) | 19 (7) | 11 (5) | 22 (8) |
| C(4) | 17 (7) | 6 (6) | 12 (8) |
| C(5) | 27 (6) | 21 (5) | 14 (7) |
| N(1) | 7 (12) | 8 (6) | 6 (5) |
| N(2) | 12 (5) | 31 (5) | 21 (8) |
| Average | ⟨17⟩ | ⟨20⟩ | ⟨16⟩ |

Table 6. *Rigid-bond tests on mean-square displacements* ($U$) (Å$^2$) *of non-hydrogen atoms along directions of adjacent bonds*

| | | Refinement II | | Refinement III | |
|---|---|---|---|---|---|
| $A$ | $B$ | $10^4\,U_{AB}$ | $10^4\,U_{BA}$ | $10^4\,U_{AB}$ | $10^4\,U_{BA}$ |
| C(1) | C(2) | 194 | 198 | 193 | 195 |
| C(2) | C(3) | 165 | 161 | 165 | 163 |
| C(4) | C(5) | 131 | 130 | 130 | 128 |
| C(3) | N(1) | 128 | 119 | 125 | 120 |
| C(4) | N(1) | 147 | 141 | 147 | 141 |
| C(5) | N(2) | 129 | 134 | 128 | 130 |
| $\sigma(U)$* | | 0·00059 Å$^2$ | | 0·00040 Å$^2$ | |

* Defined as $\{\sum_n (U_{AB} - U_{BA})^2/(n-1)\}^{1/2}$.

tained and electron density may be assigned to a relatively remote atom. This is to a lesser extent also true for the spherical harmonic expansion which gives values much larger than obtained with the 'stockholder' partitioning method (Hirshfeld, 1977*b*,*c*), the results of which are listed in the last two columns. In contrast with the original use of the stockholder concept (column *C*, Table 7) we have also applied the method to the observed dynamic density (column *D*) basing the weights in the partitioning scheme on thermally smeared free-atom densities:

$$\rho_i(\mathbf{r}) = w_i \rho_{\text{total}}(\mathbf{r}) = \frac{\langle \rho_{i,\text{ free atom}} \rangle}{\sum \langle \rho_{i,\text{ free atom}} \rangle} \rho_{\text{total}}(\mathbf{r}).$$

Though there are differences in detail between columns *C* and *D* both methods agree on the small size of the charge on the ylide carbon atom C(4), which is formally negative, showing again the lack of correlation between formal charges and the actual electron distribution. There is also agreement on the dipolar character of the cyano group with a fairly large negative charge accumulation (~0·2 e) on the cyano nitrogen.

Notwithstanding the difference between the radial functions in (1) and (2), there is some similarity between the orbital exponents from the two refinements especially for the ring carbon and nitrogen atoms (Table 8). The population parameters from the multipole expansion are more amenable to qualitative analysis than those from (1) as they refer directly to orthogonal spherical harmonic functions. They show quite large negative populations [up to −0·27 and −0·24 for C(2) and C(3), respectively] of the $d_z 2$ functions on the ring atoms, indicating a contraction of the density into the plane of the six-membered ring. Other functions with conspicuously large populations include the octapoles $f_{x^3}$ on the ring atoms, which account for much of the bond density in the trigonal arrangement of covalent bonds around these atoms.

Table 7. *Net atomic charges according to charge density parameters and stockholder concept partitioning*

*A*: from Hirshfeld formalism refinement.
*B*: from spherical harmonic refinement.
*C*: stockholder partitioning of Hirshfeld refinement static model density.
*D*: stockholder partitioning of (dynamic) experimental density.

| | *A**† | *B** | *C* | *D* |
|---|---|---|---|---|
| C(1) | −0·03 | −0·44 | 0·02 | −0·02 |
| C(2) | 0·81 | −0·45 | −0·01 | −0·06 |
| C(3) | 1·29 | −0·35 | 0·04 | −0·01 |
| C(4) | −2·01 | −0·08 | 0·00 | −0·05 |
| C(5) | −0·20 | −0·00 | 0·07 | +0·05 |
| N(1) | −1·00 | +0·06 | +0·12 | +0·06 |
| N(2) | 1·00 | −0·22 | −0·21 | −0·23 |
| D(1) | −0·55 | +0·54 | 0·04 | +0·14 |
| D(2)† | | +0·52 | 0·02 | +0·09 |
| D(3)† | | +0·49 | 0·02 | +0·09 |

* Total charge constrained to neutrality.
† Hydrogen atoms in *A* constrained to have identical charges.

*Electron density maps*

A number of electron density maps, defined in detail elsewhere (Coppens & Hansen, 1977) will be used for discussion.

(*a*) *Residual maps.* Residual maps (Fig. 2) are a measure of the adequacy of the least-squares fitting functions. Features are somewhat more pronounced in the spherical harmonic maps in accordance with the smaller number of fitting functions. But residual peaks are generally observed in the same region independent of the type of refinement. The highest (0·10–0·15 e Å$^{-3}$) are between the cyano groups and near the H(3) atom.

(*b*) $X - X_{\text{HO}}$ *maps.* $X - X_{\text{HO}}$ maps (Fig. 3) were calculated with atomic parameters obtained in a high-order refinement ($S > 0{\cdot}75$ Å$^{-1}$); with all reflections below $S = 0{\cdot}80$ Å$^{-1}$ included in the Fourier summation. They show density accumulation in all bonds and in the lone-pair region of the cyano nitrogen atom. The triple bond, C(5)≡N(1), is clearly distinguished by a large extension in the plane of the molecule perpendicular to the bond axis as has been observed, for example, in a tetracyanoethylene (Becker, Coppens & Ross, 1973). The low background noise level in these maps attests to the quality of the experimental data used in the present study. The estimated standard deviation in the map in the regions away from the atomic positions is 0·04 e Å$^{-3}$.

(*c*) *Dynamic model deformation maps.* The dynamic model deformation maps, calculated with the Fourier coefficients $F_{\text{calc, model}}(\mathbf{H}) - F_{\text{calc, spherical atom}}(\mathbf{H})$ are directly comparable with the $X - X_{\text{HO}}$ distributions. The similarities between the Hirshfeld (Fig. 4*a*) and

Table 8. *Orbital exponents* (a.u.$^{-1}$) *and kappa values*

| | Refinement II* | Refinement III† | |
|---|---|---|---|
| | $\alpha$ | $\alpha$ | $\kappa$ |
| C(1) | 5·5 (4) | 5·7 (2) | 0·970 (7) |
| C(2) | 5·5 (2) | 5·5 (1) | 0·967 (5) |
| C(3) | 6·2 (2) | 5·6 (1) | 0·983 (5) |
| C(4) | 4·3 (1) | 5·6 (2) | 0·999 (7) |
| C(5) | 5·1 (3) | 6·1 (3) | 1·012 (8) |
| N(1) | 6·1 (5) | 6·7 (4) | 1·003 (7) |
| N(2) | 5·6 (2) | 7·3 (4) | 0·995 (3) |
| D | 3·6 (2) | 4·3 (9) | 1·24 (2) |

* With the exponent of $r$ (expression 1) equal to 0, 2, 4 for monopoles; 1, 3 for dipoles; 2, 4 for quadrupoles; 3 for octapoles and 4 for hexadecapoles.
† With the exponent of $r$ (expression 2) equal to 2, 2, 3 and 4 for dipoles, quadrupoles, octapoles and hexadecapoles, respectively.

multipole model deformation maps (Fig. 4*b*) is remarkable, the peak heights in the C–C, C–H and N–C bonds and the nitrogen lone pairs being almost identical, though the peak shapes show differences. Though the bond peak heights are the same as those observed in the $X-X_{HO}$ maps, the lone-pair peak height is lower in the $X-X_{HO}$ map as a result of a low $\sin\theta/\lambda$ cut off used to eliminate background noise in the latter case. The overall agreement supports the conclusion that the charge deformation models provide a good description of the density features in this structure.

(*d*) *Static model deformation maps.* The static model deformation maps (Figs. 5 and 6) are a plot of the least-squares fitting functions minus the free-atom densities. As thermal motion is treated by a separate temperature factor the maps represent an attempt at deconvolution of thermal motion and extrapolation to infinite resolution. The method necessary leads to a distribution which is sensitive to the character of the fitting functions employed. It is therefore not surprising that the differences between the two sets of static maps are more pronounced than in the case of the dynamic distributions. The static multipole model map has sharper features and a higher peak close to the nitrogen atom in the C–N bond, while the peaks in the C–C ring bonds are, on the other hand, more regular and centered closer to the bond midpoint in multipole model maps. Such differences are a reminder that the 'pseudo' static maps are indeed model dependent.

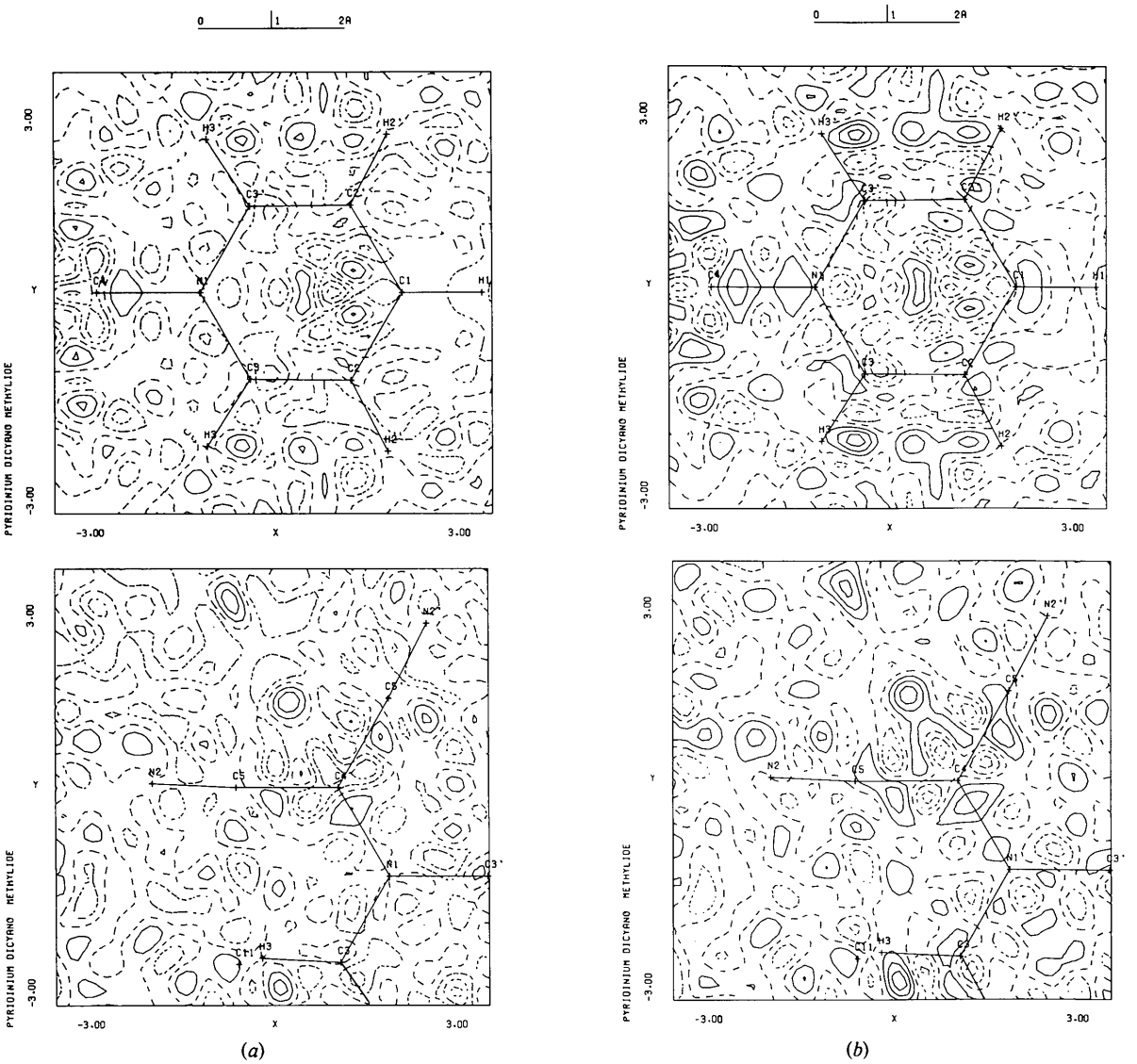


Fig. 2. Residual maps in the planes of the pyridine ring (plane $m_1$) (top) and the dicyanomethylide group (plane $m_3$) (bottom). Contours at 0·05 e Å $^{-3}$, negative contours broken. (*a*) From refinement with Hirshfeld functions; (*b*) from multipole refinement.

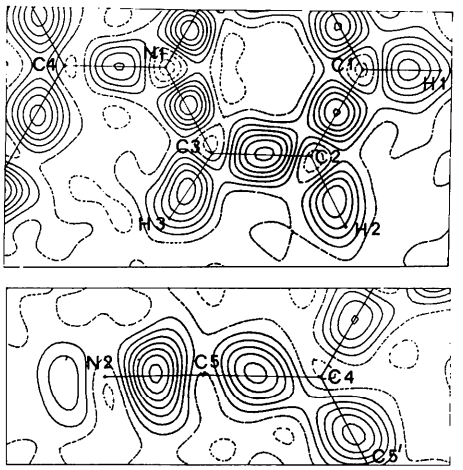


Fig. 3. $X - X_{HO}$ maps in the planes of Fig. 2. Contours at 0·10 e Å$^{-3}$, negative contours broken.

*Molecular dipole moment*

A summary of molecular dipole moments derived by different techniques is given in Table 9. The spherical harmonic refinement (II) gives a quite reasonable value which is close to the moment measured in dioxane solution by Treiner, Skinner & Fuoss (1964) and also in agreement with the value obtained by direct integration of the experimental density (Moss & Coppens, 1982). The result from the Hirshfeld refinement is surprisingly large and related to the unrealistically large net charges on the C(2), C(3) and C(4) carbon atoms. The stockholder recipe value is small in agreement with the observation by Hirshfeld & Hope (1980) that this recipe gives minimum values for the outer moments of the molecular deformation density.

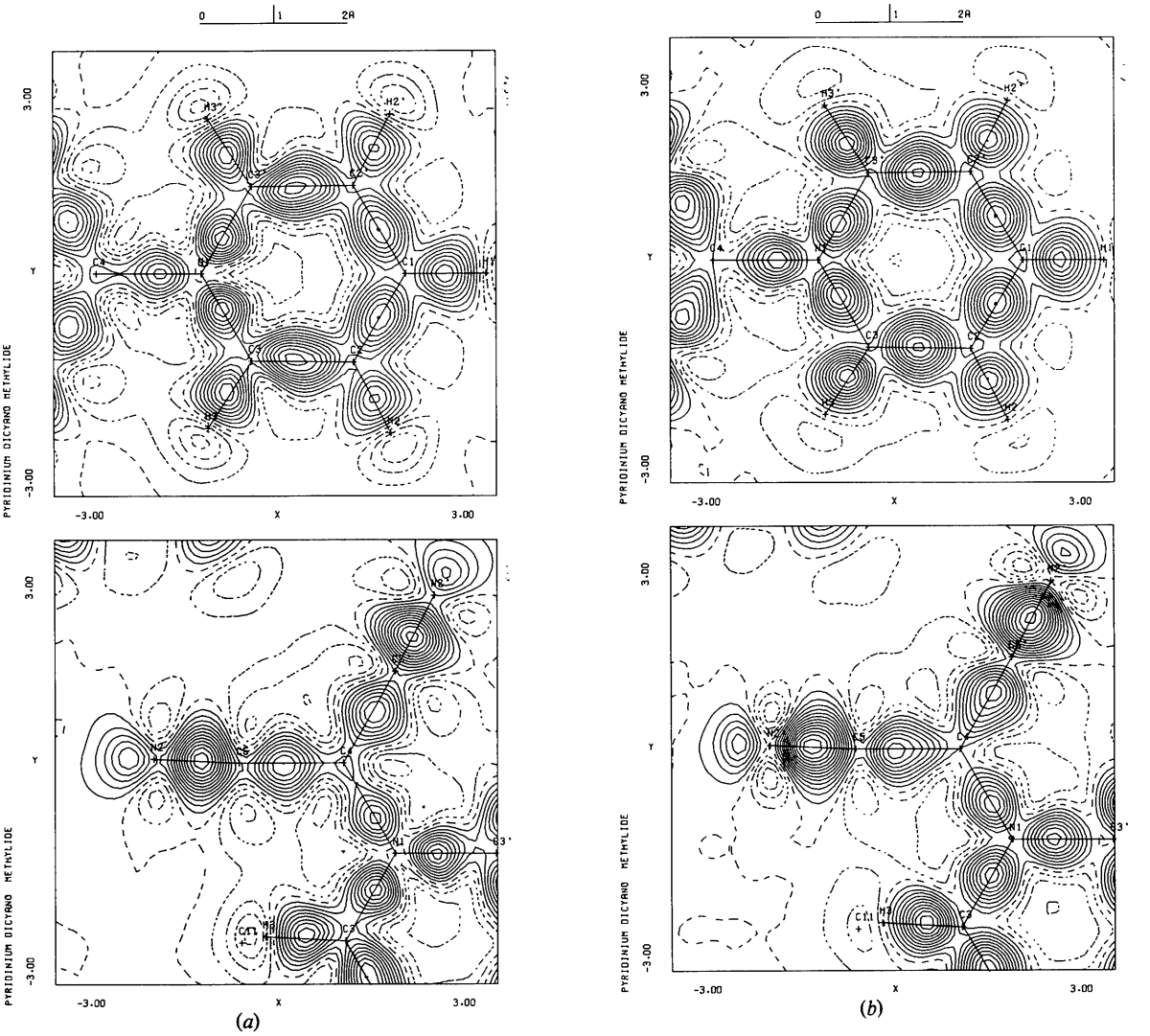


Fig. 4. Dynamic model deformation maps in the planes of Fig. 2. (*a*) From refinement with Hirshfeld functions; (*b*) from multipole refinement. Contours as in Fig. 2.

## Conclusion

Perhaps the most striking result of this comparative study is the similarity of the results obtained with both methods. The agreement factors show only small differences, positional parameters show no significant differences, while the density maps, with the exception of the pseudostatic ones, are very similar. Both methods give good agreement when the rigid-bond test is applied and neither serves well for the derivation of atomic charges. For the latter purpose other choices such as the stockholder partitioning method, or a more atom-localized treatment with monopoles only (the $\kappa$ refinement) are preferable.

Finally, it appears from this study that the spherical harmonic refinement yields the more reliable estimate of the molecular dipole moment in the crystal.

One of us (FB) would like to thank Professor F. L. Hirshfeld for his helpful suggestions and patient guidance during his stay at the Weizmann Institute. This work was supported by the National Science Foundation (CHE 7905897) and by the National Science Foundation and the Centre National de la Recherche Scientifique under the US–France exchange program.

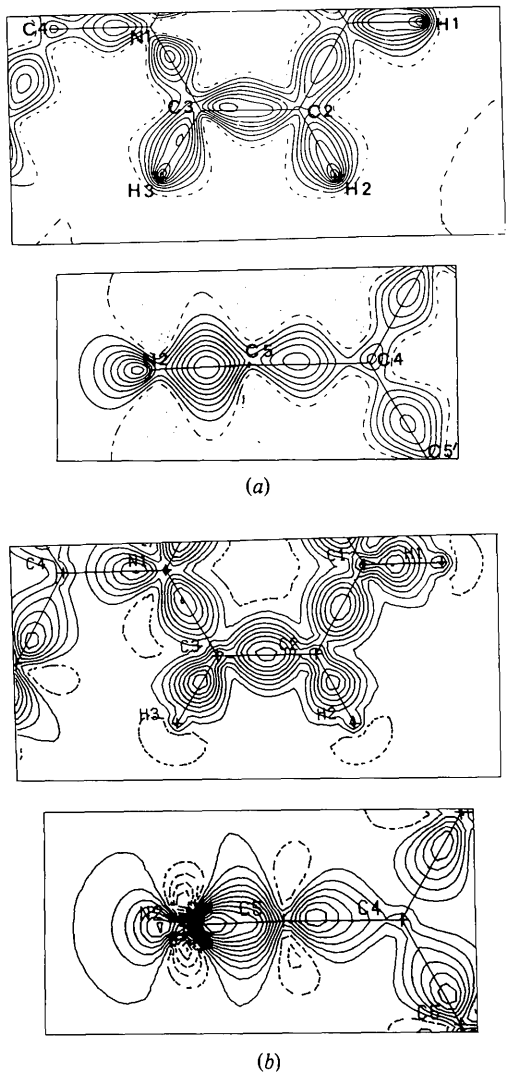


Fig. 5. Static-model deformation maps in the planes of Fig. 2. (*a*) From refinement with Hirshfeld functions; (*b*) from multipole refinement. Contours at 0·1 e Å$^{-3}$. Negative contours broken.

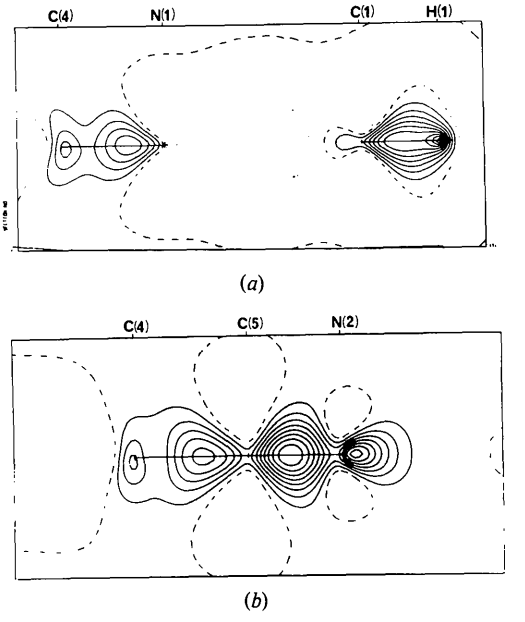


Fig. 6. Static-model deformation maps from Hirshfeld refinement. (*a*) In plane through N(1) and C(1) perpendicular to the pyridine ring (plane $m_2$); (*b*) perpendicular to the plane of the cyano group through C(4) and C(5) (plane $m_4$). Contours at 0·1 e Å$^{-3}$. Negative contours dotted, zero contour broken.

Table 9. *Summary of molecular dipole moments* ($\times 10^{-30}$ Cm)

All dipole moments have their negative pole towards cyano groups.

| | |
|---|---|
| Hirshfeld refinement* (II) | 62·7 (18·8 D) |
| Spherical harmonic refinement* (III) | 32·7 (9·8 D) |
| Direct integration† | 30·7 (9·2 D) |
| Stockholder recipe‡ | 20·0 (6·0 D) |
| Solution value§ | 30·7 (9·2 D) |

* Calculated from $\sum_{\text{all atoms}} (q_i \mathbf{r}_i + d_i)$, where $q_i$ is net charge on atom $i$ at $\mathbf{r}_i$ and $d_i$ is the atomic dipole from the $l = 1$ ($n = 1$) functions.

† Moss & Coppens (1982).

‡ Hirshfeld (1977*b*).

§ In dioxane solution (Treiner, Skinner & Fuoss, 1964).

### References

BECKER, P. & COPPENS, P. (1974). *Acta Cryst.* A**30**, 148–153.
BECKER, P., COPPENS, P. & ROSS, F. K. (1973). *J. Am. Chem. Soc.* **95**, 7604–7609.
BUGG, C. & SASS, R. L. (1965). *Acta Cryst.* **18**, 591–594.
COPPENS, P., BOEHME, R., PRICE, P. F. & STEVENS, E. D. (1981). *Acta Cryst.* A**37**, 857–863.
COPPENS, P. & HANSEN, N. L. (1977). *Isr. J. Chem.* **16**, 163–162.
DEVOS, L., BAERT, F., FOURET, R. & THOMAS, M. (1980). *Acta Cryst.* B**36**, 1807–1811.
HANSEN, N. K. & COPPENS, P. (1978). *Acta Cryst.* A**34**, 909–921.
HAREL, M. & HIRSHFELD, F. L. (1975). *Acta Cryst.* B**31**, 162–172.
HIRSHFELD, F. L. (1971). *Acta Cryst.* B**27**, 769–781.
HIRSHFELD, F. L. (1976). *Acta Cryst.* A**36**, 239–244.
HIRSHFELD, F. L. (1977*a*). *Isr. J. Chem.* **16**, 226–230.
HIRSHFELD, F. L. (1977*b*). *Theor. Chim. Acta*, **44**, 129–138.
HIRSHFELD, F. L. (1977*c*). *Isr. J. Chem.* **16**, 198–201.
HIRSHFELD, F. L. & HOPE, H. (1980). *Acta Cryst.* B**36**, 406–415.
*International Tables for X-ray Crystallography* (1962). Vol. III. Birmingham: Kynoch Press.
KURKI-SUONIO, K. (1968). *Acta Cryst.* A**24**, 379–390.
KURKI-SUONIO, K. (1977). *Isr. J. Chem.* **16**, 115–123.
MOSS, G. & COPPENS, P. (1982). In preparation.
STEVENS, E. D. & COPPENS, P. (1975). *Acta Cryst.* A**31**, 612–619.
STEWART, R. F. (1976). *Acta Cryst.* A**32**, 565–575.
STEWART, R. F., DAVIDSON, E. R. & SIMPSON, W. T. (1965). *J. Chem. Phys.* **42**, 3175–3187.
TREINER, C., SKINNER, J. F. & FUOSS, R. M. (1964). *J. Phys. Chem.* **68**, 3406–3409.


*Acta Cryst.* (1982). A**38**, 151–154

# Mechanisms for a Rapid Phase Transformation of $Nb_3Si$ from the $Ti_3P$ Structure to the $Cr_3Si$ ($A15$) Structure

BY B. W. OLINGER, L. R. NEWKIRK AND J. C. KING

*Los Alamos National Laboratory, Los Alamos, New Mexico* 87545, *USA*

(*Received* 15 *May* 1981; *accepted* 26 *August* 1981)


### Abstract

$Nb_3Si$ in the $Cr_3Si$ ($A15$) structure has been successfully recovered in bulk amounts after shock compressing $Nb_3Si$ in the $Ti_3P$ structure. The material was under compression less than 1 μs. To account for the extreme rapidity of the transformation we find that the essential characteristics of the $Cr_3Si$ structure can be achieved by screw rotating one type of column of Nb-atom pairs 45° and one quarter cell length in the $Ti_3P$ structure. It is further shown that the $Fe_3P$ structure cannot be similarly transformed.


### Introduction

We recently recovered bulk amounts of $Nb_3Si$ in the $Cr_3Si$ ($A15$) structure using dynamic high pressures generated by explosives. The lattice parameter is 5·091 ± 0·006 Å, the inductive $T_c$ is 18·6 K, it displays a large specific heat transition at 18·0 K, and has an upper critical field of 12·5 T (Olinger & Newkirk, 1981; Stewart, Olinger & Newkirk, 1981*a*,*b*).

The starting material was prepared by arc melting high-purity niobium and silicon in 3:1 atomic proportions. The alloy was then annealed in vacuum at 2048–2063 K for 3 to 5 h. X-ray powder diffraction measurements on an annealed cylinder showed it to consist primarily of the $Ti_3P$-type structure. Also, small amounts of $Nb_5Si_3$ and Nb were present. Preliminary two-dimensional hydrodynamic calculations showed that the bulk of the samples was subjected to a pressure in the range 90 to 110 GPa for less than 1 μs. The temperatures generated in the sample at the peak of the shock were of the order of 1300 K with a residual temperature of about 800 K. The amount of conversion to the $Cr_3Si$ structure was estimated from diffractometer traces to be between 50 to 75% with the residuals composed of Nb, $Nb_5Si_3$ and some $Nb_3Si$ in the $Ti_3P$ structure.

The phenomenon which prompted this study was the short time interval in which the $Ti_3P$ structure transformed into the $Cr_3Si$ structure. The 100 GPa isobar, for instance, of the shock wave passing through the sample was about 0·8 mm thick and its velocity was 8 mm/μs; thus the material remained above 100 GPa for only about 0·1 μs. It is important to know if such a transformation required diffusion across atomic planes, or required slight shifts in atomic positions. If transformations requiring diffusion could occur in such

0567-7394/82/010151-04$01.00